Coherent traveling waves in nonlocally coupled chaotic systems

Volodymyr Dziubak,[1] Yuri Maistrenko,[2,3] and Eckehard Schöll[3]
[1]*National University of Kyiv-Mohyla Academy, Skovorody Str. 2, 04655 Kiev, Ukraine*
[2]*Institute of Mathematics and Center for Medical and Biotechnical Research, National Academy of Sciences of Ukraine, Tereschenkivska Str. 3, 01601 Kiev, Ukraine*
[3]*Institut für Theoretische Physik, TU Berlin, Hardenbergstrasse 36, 10623 Berlin, Germany*
(Received 17 October 2012; revised manuscript received 28 February 2013; published 14 March 2013)

We discuss the origin of coherent traveling wave patterns in a network of coupled chaotic Lorenz systems with nonlocal interaction. By systematically analyzing the dependence of the spatiotemporal network dynamics on the range and strength of the coupling, we uncover a bifurcation scenario for the transition from stationary patterns to regular traveling waves of different wave numbers. The transition is ruled by a symmetric homoclinic bifurcation and is accompanied by the appearance of periodic and chaotic breathing, as well as long chaotic transients.

DOI: 10.1103/PhysRevE.87.032907 PACS number(s): 05.45.Gg, 05.45.Xt, 05.45.Yv

I. INTRODUCTION

Complex networks occur in a plethora of applications in physics, biology, and technology [1–3], e.g., coupled lasers, genetic or neural networks, power grids, and communication networks. The study of dynamics on networks has become a challenging paradigm as contrasted with spatiotemporal patterns on continuously extended media. Significant novel features are found when emergent spatiotemporal patterns which are well known, e.g., in spatially continuous reaction-diffusion systems described by partial differential equations, are studied on networks. Recent prominent examples are Turing patterns [4], traveling fronts [5–8], and traveling waves [9,10]. Besides completely synchronized periodic or chaotic oscillations, the phenomenon of chimera states, where a network of oscillators splits into coexisting spatial domains of coherent, phase-locked and incoherent, desynchronized behavior, has attracted much interest [11–24], but experimental evidence has been presented only very recently [25,26].

These chimera states have been shown to arise in bifurcation scenarios of networks of chaotic systems with nonlocal coupling of a variable range, during the transition from spatial coherence to incoherence [25,27,28]. Here we report a different scenario which arises in nonlocally coupled networks of chaotic elements and which leads to coherent traveling waves, whose profiles do not change over time.

II. MODEL

We consider a ring of N nonlocally coupled chaotic Lorenz oscillators

$$\begin{aligned}\dot{x}_i &= \zeta(y_i - x_i) + \frac{\sigma_x}{2P}\sum_{j=i-P}^{i+P}(x_j - x_i),\\ \dot{y}_i &= x_i(\rho - z_i) - y_i + \frac{\sigma_y}{2P}\sum_{j=i-P}^{i+P}(y_j - y_i),\\ \dot{z}_i &= x_i y_i - \beta z_i + \frac{\sigma_z}{2P}\sum_{j=i-P}^{i+P}(z_j - z_i),\end{aligned} \tag{1}$$

where x_i, y_i, z_i $(i = 1, \ldots, N)$ are real dynamic variables and the index i is periodic mod N. The positive parameters ζ, ρ, β are fixed in the chaotic regime of the uncoupled Lorenz system [29]. P specifies the number of neighbors in each direction coupled with the ith element, and σ_x, σ_y, and σ_z are the coupling strengths of the respective coordinates. First, the coupling is assumed only through the first two coordinates, x_i and y_i ($\sigma_x = \sigma_y \equiv \sigma$, $\sigma_z = 0$). However, as we demonstrate below, traveling waves exist also for more general coupling configurations.

Results of direct numerical simulation in the parameter plane of the coupling radius $r = P/N$ and the coupling strength σ are presented in Fig. 1(a). It reveals the existence of two characteristic regions tangent to each other: traveling waves of different wave numbers (different shades of yellow) and stationary patterns (different shades of blue hatching). Examples of these states for the parameters marked by $A*$ and $B*$ are illustrated in Figs. 1(b)–1(e) as snapshots (left column) and space-time plots (right column). The profiles of traveling [Fig. 1(b)] and stationary [Fig. 1(d)] patterns look similar: they are coherent and invariant under the transformation $x_i \to -x_{i+N/2}, \forall i$. The stationary pattern [Fig. 1(d)] has, in addition, an inversion symmetry $x_i = x_{2i_s - i}, \forall i$, for some i_s, which the traveling wave [Fig. 1(b)] does not have. With decreasing σ the stationary state loses its spatial coherence in a coherence-incoherence transition similar to the one found in nonlocally coupled logistic maps and Rössler systems [27,28] via chimera states.

Traveling waves are found in Fig. 1(a) for intermediate values of the coupling radius r and coupling strength σ. Only the regions for wave numbers $k = 1$, $k = 2$, and $k = 3$ are shown, although a further decrease of r yields additional, thinner high-order regions following a period-adding cascade $k = 4,5,6,\ldots$ With decreasing r the overlap of regions with different k increases, leading to a higher degree of multistability. Different wave numbers of the stationary patterns below the traveling wave region are also marked by different shades of blue hatching.

For small values of r or σ the network dynamics typically exhibits high-dimensional spatiotemporal chaos and oscillatory patterns. We emphasize that for nearest-neighboring coupling, i.e., $r = 1/N$, multistability of stationary patterns is possible, but coherent traveling waves have not been observed [30].

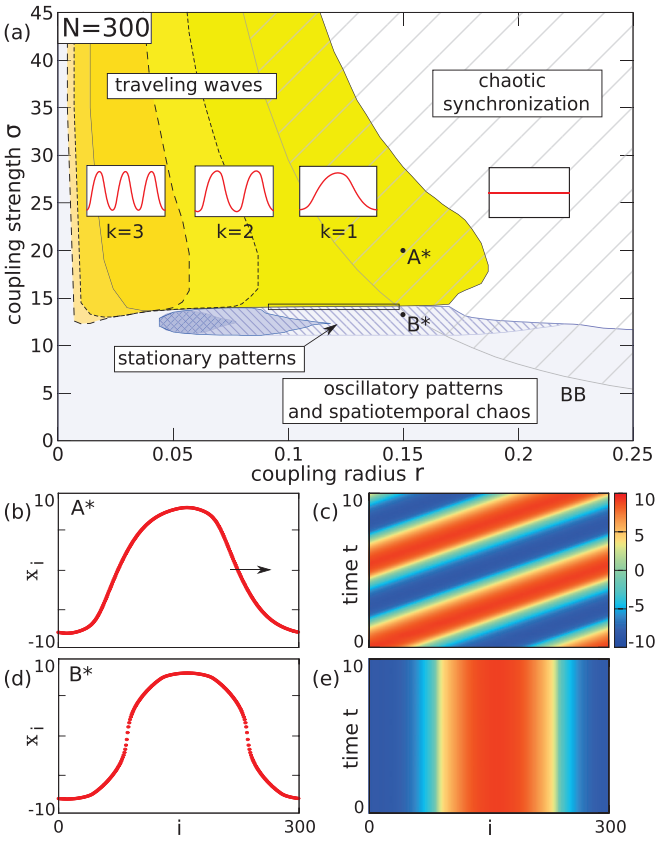

FIG. 1. (Color online) (a) Different dynamical regimes in the (r,σ) parameter plane. Coherent traveling waves are labeled with wave numbers $k = 1,2,3$. Snapshots of typical wave shapes are shown for x_i in the insets. The completely synchronized chaotic state exists in the gray hatched region bounded by the blowout bifurcation curve BB. (b) Snapshot x_i and (c) space-time plot of traveling waves ($r = 0.15$, $\sigma = 20$) and (d) and (e) the same plots for stationary patterns ($r = 0.15$, $\sigma = 13.5$). Parameters are $\zeta = 10$, $\rho = 28$, $\beta = 8/3$, $N = 300$, $\sigma_x = \sigma_y \equiv \sigma$, $\sigma_z = 0$.

At the opposite end of the bifurcation diagram, where r and σ are large enough, chaotic synchronization occurs: the oscillators in the network behave identically in space but chaotically in time following the strange attractor of a single Lorenz system. In Fig. 1(a), the region of chaotic synchronization is hatched in light gray, being bounded by the blowout bifurcation curve (BB), where the maximum transverse Lyapunov exponent of the synchronized state becomes positive and chaotic synchronization is no longer stable. The chaotic synchronization region partially overlaps with both traveling waves and stationary patterns, causing multistability. For very large σ, the traveling wave region shrinks proportionally to $1/r$, and the only stable regime left is chaotic synchronization.

Our numerical simulations show that traveling waves persist also for more general coupling configurations in Eq. (1). This is illustrated in Fig. 2 where the parameter regimes for the existence of traveling waves ($k = 1$) are depicted for coupling coefficients perturbed as follows: $\sigma_x = \sigma + \Delta\sigma_x$, $\sigma_y = \sigma$, $\sigma_z = \Delta\sigma_z$. We find that the shape of the wave is similar to

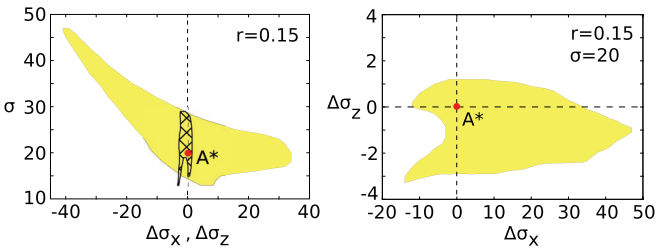

FIG. 2. (Color online) Regimes of traveling waves for more general coupling configurations: $\sigma_x = \sigma + \Delta\sigma_x$, $\sigma_y = \sigma$, $\sigma_z = \Delta\sigma_z$. (a) σ vs $\Delta\sigma_x$ for $\Delta\sigma_z = 0$ (yellow shading) and σ vs $\Delta\sigma_z$ for $\Delta\sigma_x = 0$ (hatched area); (b) $\Delta\sigma_z$ vs $\Delta\sigma_x$ for $\sigma = 20$, $r = 0.15$ [point $A*$ in Fig. 1(a)]. Other parameters as in Fig. 1.

that illustrated in Fig. 1(b), but it becomes more asymmetric with increasing coupling asymmetry $\Delta\sigma_x$ and $\Delta\sigma_z$.

III. BIFURCATION SCENARIOS

Next, we will investigate the bifurcation scenarios from stationary patterns to traveling waves. The detailed structure of the various transition regimes in the (r,σ) parameter space is shown in Figs. 3(a)–3(c) for $N = 300$, $N = 200$, and $N = 100$, respectively. With decreasing system size N the width of these transition regimes between stationary patterns (SP) and traveling waves (TW_1) grows substantially. Also, with decreasing coupling range r the transition regime widens and undergoes essential changes. Different bifurcation scenarios, denoted by sc_1, sc_2, and sc_3, are marked by vertical lines in the (r,σ) space.

For large N and r the transition along line sc_1 [Fig. 3(a)] with increasing σ starts with a saddle-node bifurcation of a pair of stable (TW_1, yellow region) and unstable traveling waves at the red dashed line, followed by a subcritical Hopf destabilization of the stationary pattern (solid blue line). Including bistability and hysteresis, it represents a typical bifurcation scenario for traveling fronts and waves in discrete systems, e.g., locally coupled FitzHugh-Nagumo oscillators [8], and continuous media [31,32]. It is schematically shown in Fig. 4(a).

With decreasing N and r, the complexity of the transition grows, as shown schematically in Fig. 4(b) [e.g., line sc_2 in Fig. 3(b)]. It includes a supercritical Hopf bifurcation (H) of the stationary pattern, giving rise to small-amplitude breathing (SBr, green region in Fig. 3). An example of the breathing behavior is illustrated in Fig. 5(g). Upon a further increase of σ, the breathing amplitude grows, and a homoclinic bifurcation occurs when two breathing limit cycles with a phase lag of π (two antiphase oscillations) simultaneously collide with a saddle-point (stationary pattern) S forming a double homoclinic orbit attached to this saddle point. This is a "gluing" bifurcation, where two neighboring breathing patterns (i.e., two patterns which are shifted on the ring by one element) coalesce at $x = 0$. It generates a second traveling wave, denoted by TW_2 (orange region in Fig. 3). The spatial profile of TW_2 is similar to that of TW_1. However, closer to the homoclinic bifurcation point, the profile of TW_2 looks more and more symmetric, and the wave velocity tends to zero,

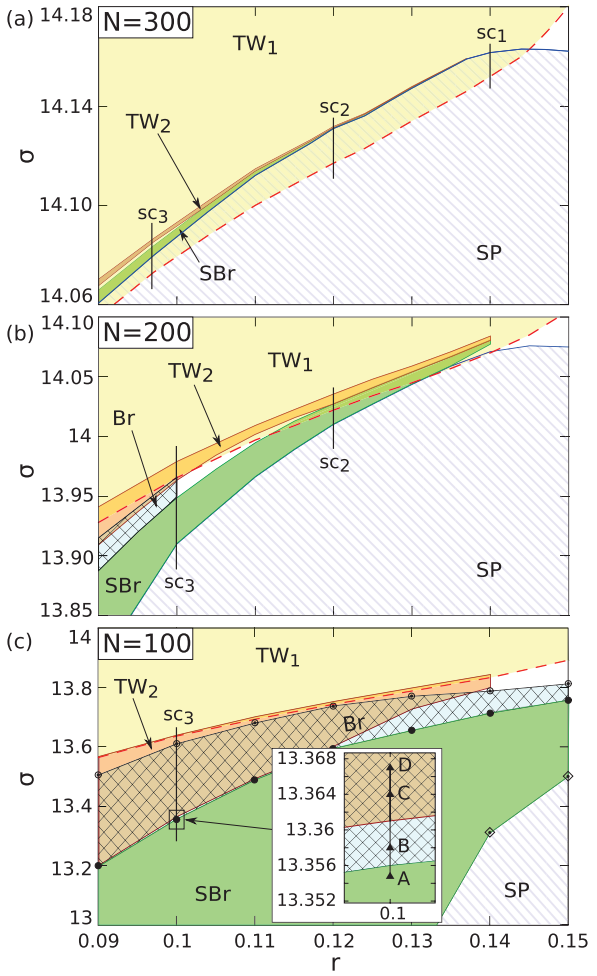

FIG. 3. (Color online) Transitions from stationary patterns to traveling waves in the (r,σ) parameter plane for (a) $N = 300$, (b) $N = 200$, (c) and $N = 100$ chaotic Lorenz oscillators. Different dynamic regimes are given by yellow shading (traveling waves TW_1), orange shading (traveling waves TW_2), dark blue squares (breathing Br), green shading (small-amplitude breathing SBr), and light blue hatching (stationary patterns SP). Different bifurcation scenarios are marked by vertical lines sc_1, sc_2, and sc_3. (a) corresponds to a blowup of the thin rectangle marked in Fig. 1(a) between the traveling wave and the stationary pattern regions. Parameters are as in Fig. 1.

manifesting the logarithmic scaling law of its round-trip period in the ring. This is scenario sc_2, which takes place, e.g., for $N = 300$ or 200 and $r = 0.12$. It is similar to the origin of discrete traveling waves in arrays of globally coupled Josephson junctions (ponies on a merry-go-round) [33] and traveling fronts in locally coupled bistable Lorenz systems [5,7,8].

With a further decrease of N and r the transition becomes even more complicated; see scenario sc_3 in Fig. 3(c), which is depicted schematically in Fig. 4(c). In Fig. 5 the bifurcation scenario is illustrated for $N = 100$ oscillators, where we fix the coupling range $r = 0.1$ and sweep the coupling strength σ up from A to D along the triangles on the vertical line in the inset of Fig. 3(c).

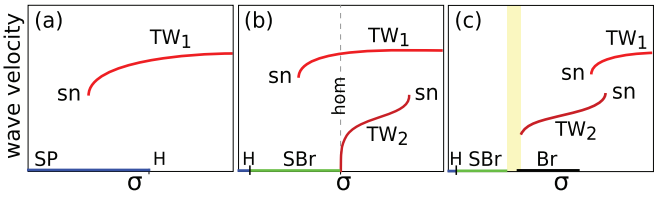

FIG. 4. (Color online) Schematic bifurcation scenarios (a) sc_1, (b) sc_2, and (c) sc_3 for the transition from stationary patterns (SP) to traveling waves (TW) as a function of the coupling strength σ: saddle-node bifurcation (sn), Hopf bifurcation (H), homoclinic bifurcation (hom), and breathing (Br).

For better illustration, following [5], we introduce reduced cylindrical coordinates:

$$\xi_j = \frac{1}{\sqrt{2}} \sum_{i_1 \leqslant i < i_2} \left[x_i + y_i + \frac{\sigma}{8P\zeta} \sum_{l=i-P}^{i+P} (x_l - x_i) \right] \mod [2\sqrt{2\beta(\rho-1)}],$$

$$\eta_j = \frac{1}{\sqrt{2}} \sum_{i_2 \leqslant i < i_1} \left[-x_i + y_i + \frac{\sigma}{2P\zeta} \sum_{l=i-P}^{i+P} (x_l - x_i) \right], \quad (2)$$

where the subscripts $j = 1$ and $j = 2$ stand for the trailing and the leading fronts of the wave profile, respectively, assuming $k = 1$, and i_1,i_2 correspond to the positions of the minimum

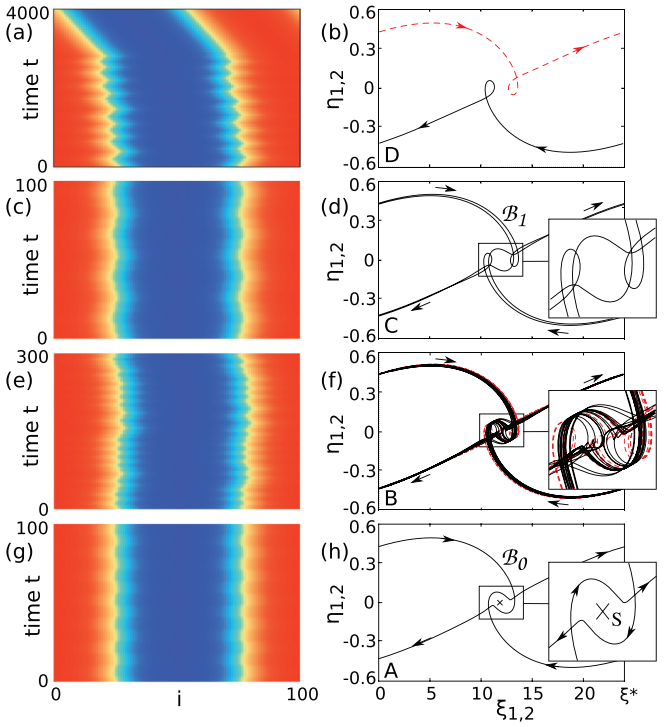

FIG. 5. (Color online) Bifurcation scenario from oscillatory states to traveling waves along line sc_3 in Fig. 3(c) ($N = 100$, $r = 0.1$). The panels from bottom to top correspond to points marked A, B, C, and D in the inset of Fig. 3(c) with values of σ = 13.355, 13.358, 13.364, and 13.367, respectively. For each value of the coupling parameter σ (left) space-time plots of x_i and (right) phase portraits (ξ_1,η_1: solid black lines; ξ_2,η_2: dashed red lines) are shown. (a) includes the transient, but in (b) (point D) only the asymptotic traveling wave is depicted.

and the maximum of the x profile (all indices mod N); see Fig. 1(b). The right column in Fig. 5 shows phase portraits in these coordinates.

If the front profiles have an inversion symmetry with respect to each other as in Fig. 1(d), then coordinates $\xi_j(t)$ and $\eta_j(t)$ for $j = 1$ and $j = 2$ coincide, as in Figs. 5(c), 5(d), 5(g), and 5(h). Alternatively, in the asymmetric case [Figs. 5(e) and 5(f)], the coordinates are different, and the difference can serve as a measure of mismatch between the left- and the right-hand front profiles of the wave.

In the (ξ_j,η_j) coordinates, the stationary pattern is a stable fixed point, while small-amplitude breathing is represented by a symmetric limit cycle $\mathcal{B}_0$; see Figs. 5(g) and 5(h). As σ is increased, the cycle $\mathcal{B}_0$ loses stability in a pitchfork bifurcation, and two asymmetric limit cycles $\mathcal{B}_0^+$ and $\mathcal{B}_0^-$ are born.

The cycles $\mathcal{B}_0^+$ and $\mathcal{B}_0^-$ grow in size, approaching the saddle point S. But, in contrast to scenario sc_2 [Fig. 4(b)], they do not disappear in a gluing homoclinic bifurcation of S. Instead, they both coalesce in an inverse saddle-node bifurcation. The homoclinic loop is not created in this case. As a result, traveling wave TW_2 is born later on in a saddle-node bifurcation. This parameter gap between the periodic small-amplitude breathing and traveling wave TW_2 is an essential property of scenario sc_3 [shown as yellow shading in Fig. 4(c)]. In the gap, the previously simple behavior (given by a pair of stable limit cycles, $\mathcal{B}_0^+$ and $\mathcal{B}_0^-$) will instead display spatiotemporal chaos. The breathing is not periodic any longer, and instead, the left- and the right-hand wave fronts move chaotically and asymmetrically [Figs. 5(e) and 5(f)]. (See the Appendix for a more detailed bifurcation analysis of scenario sc_3.)

The second peculiarity of scenario sc_3 is the appearance of large-amplitude breathing, given by periodic orbits $\mathcal{B}_l, l = 1,\ldots,l^*$. Each of the cycles is characterized by the number l of turns (loops) which its trajectory $[\xi_j(t),\eta_j(t)]$ performs around the cylinder before it reverses and starts propagating in the opposite direction. For the respective breathing states of the network, the loop number l shows how many oscillator pairs cross the $x = 0$ level in one period.

The stability intervals of the l-loop breathing states are bounded by regions of chaotic breathing transients; see Figs. 5(a) and 5(b). The asymptotic states are traveling waves or complete synchronization [above the blowout bifurcation curve (BB) shown in Fig. 1(a)]. The transient time can be very long; it grows exponentially with N, as well as with decreasing σ.

IV. CONCLUSION

In summary, we have shown the existence of coherent traveling waves in a ring network of symmetrically coupled chaotic Lorenz oscillators. These regular waves exist in a wide range of parameters in spite of strong chaoticity of the individual oscillators. Moreover, traveling waves are robust with respect to changes in the coupling scheme, e.g., asymmetries in the coupling strengths of the different components. Such behavior is caused by the nonlocal coupling of the network; it has been found neither for local (nearest-neighboring) nor for global (mean-field) coupling topologies. We have also identified a mechanism for the transition from stationary to traveling patterns, given by scenario sc_3. It consists of the appearance of periodic and chaotic breathing in a narrow parameter gap which exists prior to the traveling waves. The mechanism of the transition appears to be a finite-size effect: the parameter gap of the coupling strength shrinks with increasing network size N. We expect that the coherent traveling wave structures and their bifurcation mechanism are a rather general phenomenon and occur in other dynamical networks with nonlocal coupling.

ACKNOWLEDGMENT

We thank Diego Pazo, Arkady Pikovsky, and Michael Zaks for illuminating discussions. This work was supported by DFG in the framework of SFB 910. V.D. and Y.M. acknowledge the hospitality of TU Berlin.

APPENDIX: BIFURCATION ANALYSIS OF THE l-LOOP BREATHING STATES IN SCENARIO SC_3

Here we discuss bifurcation scenario sc_3 of Fig. 4(c) [Fig. 6(a)] in more detail. The stability intervals of σ for breathing states with different loop numbers l are shown in Fig. 6(b). The closest to the "chaotic gap" (yellow) is the "one-loop" interval, where the $\mathcal{B}_1$ cycle exists [Figs. 5(c) and 5(d)]. The one-loop cycle $\mathcal{B}_1$ is born in a saddle-node bifurcation at the right-hand end point of the interval. In the major part of the interval the breathing state is symmetric: its left- and right-hand fronts oscillate in synchrony. With decreasing σ, the symmetry is broken in a pitchfork bifurcation [shown schematically in Fig. 6(b)]. Two asymmetric one-loop cycles, $\mathcal{B}_1^+$ and $\mathcal{B}_1^-$, are born, and soon after, they cease to exist at the left edge of the interval. The bifurcation structure inside

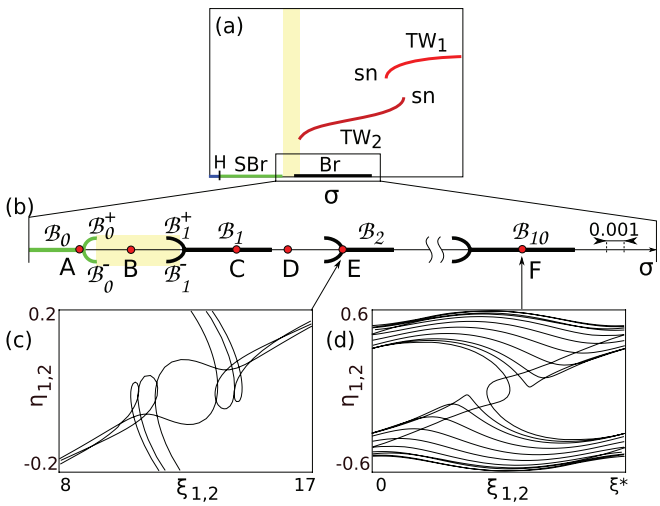

FIG. 6. (Color online) (a) Schematic bifurcation scenario sc_3 for the transition from stationary patterns (below H) to traveling waves (TW) via small-amplitude breathing (SBr), chaotic behavior (yellow stripe), and large-amplitude breathing (Br) as a function of the coupling strength σ: Hopf bifurcation (H) and saddle-node bifurcations (sn). (b) Blowup of the breathing (Br) scenario in (a) showing the stability intervals for l-loop breathing cycles $\mathcal{B}_l$, $l = 0$, 1, 2, and 10. (c) and (d) Examples of two- and ten-loop cycles, $\mathcal{B}_2$ and $\mathcal{B}_{10}$, respectively, in the (ξ_j,η_j) coordinates given by Eq. (2). Parameters are $\sigma = 13.370$ (c), 13.606 (d), $r = 0.1$, $N = 100$.

the other l-loop intervals is similar, as shown schematically in Fig. 6(b). Examples of two-loop and ten-loop cycles are illustrated in Figs. 6(c) and 6(d), respectively. For $N = 100$, $r = 0.1$ we have only found at most $l^* = 10$ l-loop intervals. With decreasing r the number of l-loop cycles grows, e.g., $l^* = 15$ for $N = 100$ and $r = 0.09$.

[1] R. Albert and A.-L. Barabási, Rev. Mod. Phys. **74**, 47 (2002).
[2] M. E. J. Newman, SIAM Rev. **45**, 167 (2003).
[3] S. Boccaletti, V. Latora, Y. Moreno, M. Chavez, and D. U. Hwang, Phys. Rep. **424**, 175 (2006).
[4] H. Nakao and A. S. Mikhailov, Nat. Phys. **6**, 544 (2010).
[5] D. Pazó and V. Pérez-Muñuzuri, Phys. Rev. E **64**, 065203(R) (2001).
[6] D. Pazó, N. Montejo, and V. Pérez-Muñuzuri, Phys. Rev. E **63**, 066206 (2001).
[7] D. Pazó and V. Pérez-Muñuzuri, Chaos **13**, 812 (2003).
[8] D. Pazó, R. R. Deza, and V. Pérez-Muñuzuri, Phys. Lett. A **340**, 132 (2005).
[9] G. C. Sethia and A. Sen, Phys. Rev. E **84**, 066203 (2011).
[10] N. Kouvaris, H. Kori, and A. S. Mikhailov, PLoS ONE 7, e45029 (2012).
[11] T. Kuroda, S. Sanguinetti, M. Gurioli, K. Watanabe, F. Minami, and N. Koguchi, Phys. Rev. B **66**, 121302 (2002).
[12] D. M. Abrams and S. H. Strogatz, Phys. Rev. Lett. **93**, 174102 (2004).
[13] D. M. Abrams, R. Mirollo, S. H. Strogatz, and D. A. Wiley, Phys. Rev. Lett. **101**, 084103 (2008).
[14] O. E. Omel'chenko, Y. L. Maistrenko, and P. A. Tass, Phys. Rev. Lett. **100**, 044105 (2008).
[15] C. R. Laing, Physica D **238**, 1569 (2009).
[16] C. R. Laing, Chaos **19**, 013113 (2009).
[17] E. A. Martens, C. R. Laing, and S. H. Strogatz, Phys. Rev. Lett. **104**, 044101 (2010).
[18] E. A. Martens, Phys. Rev. E **82**, 016216 (2010).
[19] G. Bordyugov, A. Pikovsky, and M. G. Rosenblum, Phys. Rev. E **82**, 035205 (2010).
[20] M. Wolfrum and O. E. Omel'chenko, Phys. Rev. E **84**, 015201 (2011).
[21] M. Wolfrum, O. E. Omel'chenko, S. Yanchuk, and Y. L. Maistrenko, Chaos **21**, 013112 (2011).
[22] W. S. Lee, J. G. Restrepo, E. Ott, and T. M. Antonsen, Chaos **21**, 023122 (2011).
[23] C. R. Laing, Physica D **240**, 1960 (2011).
[24] R. Singh, S. Dasgupta, and S. Sinha, Europhys. Lett. **95**, 10004 (2011).
[25] A. Hagerstrom, T. E. Murphy, R. Roy, P. Hövel, I. Omelchenko, and E. Schöll, Nat. Phys. **8**, 658 (2012).
[26] M. R. Tinsley, S. Nkomo, and K. Showalter, Nat. Phys. **8**, 662 (2012).
[27] I. Omelchenko, Y. L. Maistrenko, P. Hövel, and E. Schöll, Phys. Rev. Lett. **106**, 234102 (2011).
[28] I. Omelchenko, B. Riemenschneider, P. Hövel, Y. L. Maistrenko, and E. Schöll, Phys. Rev. E **85**, 026212 (2012).
[29] E. N. Lorenz, J. Atmos. Sci. **20**, 130 (1963).
[30] K. Josić and C. E. Wayne, J. Stat. Phys. **98**, 1 (2000).
[31] M. C. Cross and P. C. Hohenberg, Rev. Mod. Phys. **65**, 851 (1993).
[32] A. Hagberg and E. Meron, Nonlinearity **7**, 805 (1994).
[33] D. G. Aronson, M. Golubitsky, and J. Mallet-Paret, Nonlinearity **4**, 861 (1991).